

# We are IntechOpen, the world's leading publisher of Open Access books Built by scientists, for scientists

**4,800**

Open access books available

**122,000**

International authors and editors

**135M**

Downloads

Our authors are among the

**154**

Countries delivered to

**TOP 1%**

most cited scientists

**12.2%**

Contributors from top 500 universities



**WEB OF SCIENCE™**

Selection of our books indexed in the Book Citation Index  
in Web of Science™ Core Collection (BKCI)

Interested in publishing with us?  
Contact [book.department@intechopen.com](mailto:book.department@intechopen.com)

Numbers displayed above are based on latest data collected.

For more information visit [www.intechopen.com](http://www.intechopen.com)



# Optical Coherence Tomography in Dentistry

Yueli L. Chen<sup>1</sup>, Quan Zhang<sup>2</sup> and Quing Zhu<sup>1</sup>

<sup>1</sup>*Biomedical Engineering Department, University of Connecticut, Storrs,*

<sup>2</sup>*Massachusetts General Hospital, Harvard Medical School, Charlestown, MA  
USA*

## 1. Introduction

Optical Coherence Tomography is an imaging technique characterized by high spatial resolution and noninvasive subsurface detection<sup>1</sup>. OCT started as an interferometric technique utilizing the newly emerged low coherence or partial coherence light source and time-domain gating to achieve the depth resolution. With additional lateral scans, 2-D or 3-D tomographic images can be obtained. The instrumental development of OCT has experienced several phases. It goes from free space architectures to fiber-based systems, from intensity-based structural imaging to multiple functional extensions of polarization sensitive, Doppler, and spectroscopic OCT. Since the beginning of this century, a Fourier domain OCT infrastructure has been introduced that resulted in a new revolution in OCT technology<sup>2-3</sup>. Not only was the new technology bringing a hundred times more sensitivity, it was also technically more convenient for the design of a higher speed scanning system structures. Nowadays, FD-OCT are implemented with either a spectrometer or a tunable laser design. Modern OCT is more accurately defined as a broadband rather than low-coherence interferometric technology. And the outcome is a true 3D imaging modality<sup>4-9</sup> with high data speed for real-time clinical diagnosis, free from the degradation of motion artifacts.

Bearing a two-decade history of fast pace research and development, OCT has established itself as a promising *in vivo* biomedical imaging modality. Constant efforts toward improving this imaging technology lead to more than 5000 journal publications. There is now a clear trend of extended interests towards the application side in addition to the technology development. Currently, the well established ophthalmic diagnostic application occupies about 50% of academic and industrial shares in OCT business<sup>10-19</sup>. Cardiovascular imaging<sup>20-27</sup> has become the next big thing when the coronary OCT products have seen FDA clearance in the United States. Besides the two types of applications, OCT holds promise in dermatological<sup>8, 28-31</sup>, dental<sup>32-43</sup>, small animal<sup>44-46</sup>, development biology<sup>47-49</sup>, and various endoscopic applications<sup>50-55</sup> such as for esophagus, colon, and ovarian imaging.

The focus of this chapter is on dental imaging. We will review the dental diagnostic approaches and discuss the clutching points where optical coherence tomography can seek contribution. The OCT technological prospective will be cut short in this chapter. A rich compilation of imaging figures will be present in such that readers with more application expertise may define the region of interests beyond the written text.

## 2. Traditional dental diagnosis and the limiting factors

Currently, the “gold standard” clinical diagnostic product for tooth diagnostics is dental radiography (X-ray). Although generally accepted by dental clinic, it has several imaging limitations, primarily, *the resolution and the contrast*. Dental X-ray has limited resolution. Dental X-ray images relatively smaller dental tissues compared to other applications such as chest X-ray and mammography. As a result, X-ray is not good at detecting from small tooth tissue even smaller lesions such as tiny precaries and cracks. Dental X-ray has limited imaging contrast. X-ray contrast arises from attenuation variation between different tissue composites. Human tooth consists of primarily enamel, dentin, and pulp which do not show strong X-ray contrast. Demineralization, as a major tooth decay indicator produces only subtle changes in image contrast that trained eye can tell. Believe it or not, standard diagnosis device would leave as much as 50 percent of tooth decay go undetected. To assess the tooth health, it is important to understand the microstructures, their mineralization level, and in particular the dynamic mineral exchanges within the dental tissues. High resolution imaging techniques such as AFM and TEM are used to investigate the microstructures of teeth. These studies however, can only perform under *ex vivo* scenario which is not able to clinically assess the status of the human dental health.

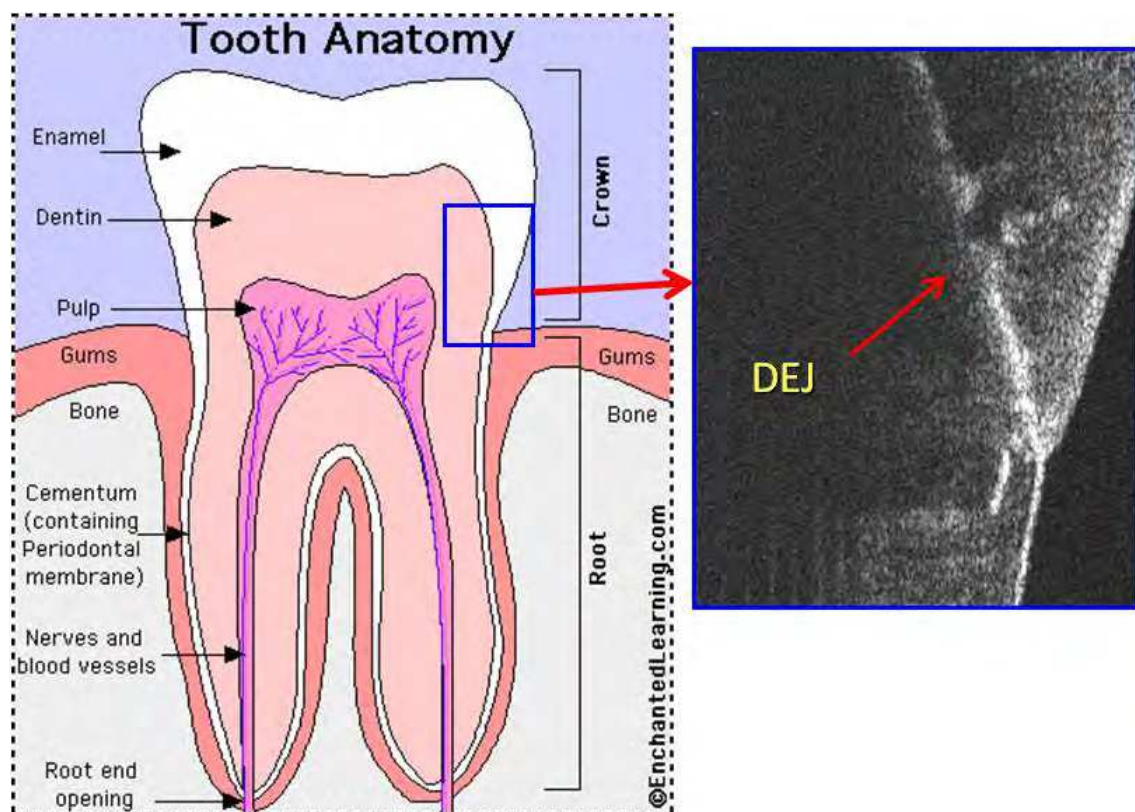


Fig. 1. The tooth anatomy. The primary components of a tooth are dentin and enamel. To the right side is an OCT B-scan (2D image), with which we can find the corresponding anatomic dental structure. This OCT image is oriented in such to get the general readers some salt on how to interpret the output of an OCT scan.

In particular, dental X-ray is not good at identify occlusal (the biting surface) cavities. As a projection method that overlaps the full volume along X-ray photon travel directions into

one 2D image, the method fell short to detect occlusal cavities. Because the X-ray takes tooth scan from the side of the tooth, this orientation effectively hides the pit or valley cavities from the dentist's view. In the past, tooth cavities are primarily developed between teeth. As the use of fluoride became more widespread, the outer tooth became strengthened. Flossing also helps removing plaques and bacterial infections hiding between the gaps of teeth. Nowadays, it is actually the canyon-like topological chewing surface that cavity most likely to develop. Bacteria can accumulate especially around the sites of the pits and valleys, the weak spots where the plaques are relatively difficult to be brushed away. As health care keeps improving, early diagnosis becomes a favorite subject in dentistry. If we can spot tiny tooth decay in an early stage, rehabilitation procedures are possible to cure the lesion and before it goes to the wrong way.

### 3. What optical coherence tomography brings to the table

Dental OCT directly addresses the image quality issue with its intrinsic high resolution and contrast mechanism, which is useful to indentify tiny precaries and fissure lesions before their potential progression to serious dental decay. As a functional extension, polarization sensitive OCT is found to be especially interesting in dental imaging. It provides unique contrast beyond regular OCT's intensity contrast from the variation of tissue materials and boundaries. We will present data to show evidence that the cavity decay responses to the polarization states of the probing light.

OCT is now typically designed as a fiber system. Therefore a flexible handheld fiber-guided probe with light weight can be fabricated for clinical purpose. The probe will facilitate a small scanner head for doctors to directly aim at regions of interests of patient's teeth. Towards commercialization, OCT probe can sit near the dentist's tool-box just as other wired gadgets. OCT also has significant advantages due to its use of cheaper and much safer near infrared light rather than radioactive source for detection. Moreover, recent advance of OCT from time-domain to Fourier domain enhanced imaging sensitivity to another 100 times. The sensitivity advantage is transferred to high-speed dental imaging acquisition *in vivo*, which is an important prospective in dental clinic practice. When imaging a non-stationary target, i.e. a patient, high speed is required to reduce the motion smearing and thus retain the high resolution property of the imager. Meanwhile, shorter scan duration is necessary to reduce the discomfort of patients especially children. Current state of the art OCT scanning speed would enable a single scan of one tooth surface within a couple of seconds. With such an imaging paradigm, we have a true 3D dental scan to cover the full surface area of teeth. This opens options for more quantitative and comprehensive diagnostic approaches, for which we will be discussing in the later section.

#### 3.1 Intensity based dental OCT

Intensity OCT images are mapped by the coherently mixed light fields between sample and reference arms where the detected signal is representing the amount of back scattered light from some certain depths of the tissue. Structural boundaries or regional optical scatterers bring different back scattering signal strength. Therefore intensity OCT primarily reveals the enfolded structural information of the imaging target. For soft tissues, OCT's penetration is usually 1-2 mm before the signal is attenuated to the noise floor. For dental tissue however, the light penetration can goes deeper to beyond 4 mm defined by optical path length in air.

This depth is achieved in our imaging system when a small numerical aperture was applied in the sample arm to increase the range of the depth of focus (DOF). The trade-off is a decrease of lateral resolution to larger than 20 micrometers. This depth range could cover the area of interests where tooth decay happens. The typical OCT resolution ranges from a few micrometers to more than ten micrometers, which is overkill to resolve a clinically significant tooth decay spot.

Figure 2 shows some typical dental OCT scans. With 256 gray scale mapping, the stronger signals are corresponding to whiter colors. The top air regions above the tooth surfaces are basically black because there is no back scattering light signal. Fig. 2A (premolar) and B (molar) are scans along the occlusal direction, meaning the scanner is pointing at the occlusal surface. In contrast to the projectile geometry of dental X-ray scans, where the images planes are perpendicular to the X-ray photon travel directions, the OCT B-scans are in the same planes of the near infrared optical photon probing trajectories. Therefore what we see from the black-white boundaries in Fig.2 A and B are in fact the topologies of the biting surfaces of the teeth. The whitish area pointed by two white arrows in Fig. 2 B likely could be signs of tooth decay.

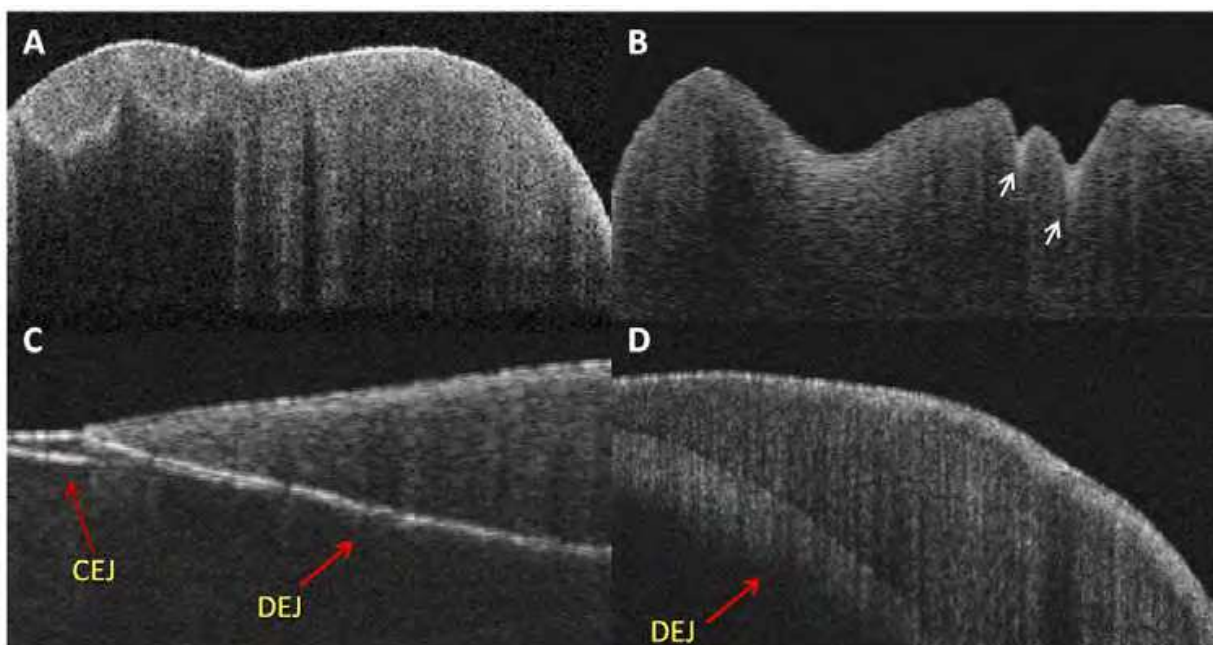


Fig. 2. Four typical intensity based OCT B-scans. A and B imaging from the occlusal direction of a premolar and molar tooth. C and D: scanning of teeth from the peripheral directions where the boundaries of dentin, enamel, and cementum can be seen. The four images are from three different systems. Therefore some system-dependent differences can be seen such as in contrast and noise levels. They are representative illustrations with different imaging scales.

The occlusal decay as mentioned earlier, is the most difficult to identify in X-ray diagnosis due to the projection of the full tooth thickness along lingual to facial direction. Even when a spurious tooth decay is spotted, it is also hard to determine the exact location of the lesion. OCT instead are capable of pinpointing the exact lesion sites. The two white arrows point to the pit areas, where bacterial infections are more likely to happen. Fig. 2C and D are scans

from the side of teeth. Fig. 2C is more close to the root and Fig. 2D more close to the crown. The dentinoenamel junction (DEJ) and the cementoenamel junction (CEJ) are clearly visible in Fig. 2C as brighter boundaries. In Fig. 2D, the boundary can be roughly differentiated with the different imaging properties of dentin (weak) and enamel (strong) tissues. There is however not a specific white band associating with the junction. On the contrary, a dark line is indentified along the boundary area. The dark area in OCT indicates lacking of tissue scattering. In our dry dental hard tissue sample, it is most likely associated with an air gap. In fact, there appears to be some other less visible crack lines in the enamel. These microstructural features are difficult to be seen in X-ray due to the resolution and contrast limitations.

Early tooth decay, even at the surface of a tooth, may not be easy to be identified by a naked eye. Sometimes, the lesion could look whiter rather than browner associated with early demineralization. Up to this point, it is clear that OCT would have ample resolution to spot tiny lesions. OCT will also have the capability to locate the position of the lesions accurately. What important next, is thus to explore if there exists a clear contrast mechanism or marker to associate with the tooth decay, and especially in the early stage. This is by far still an ongoing research topic. From Fig.3, it appears the scattering intensity itself could potentially be a marker for the tooth decay. As can be seen from the referenced photo picture to the right side, the OCT B-scan goes across a lesion spot which most likely is caused by demineralization. The lesion spot shows significantly stronger signal intensity. This is coincident with the whitish spots at the pit areas of the Fig. 2B which likely are the lesion areas associated with decay too. There is also another decay marker discussed by Choo-Smith et al<sup>56</sup>. She has used OCT attenuation slope to characterize the healthiness of a tooth. It is possible that the two types of markers may originate from the same biophysical mechanism: that the demineralization process increases the light back scattering intensity into deeper imaging depth.

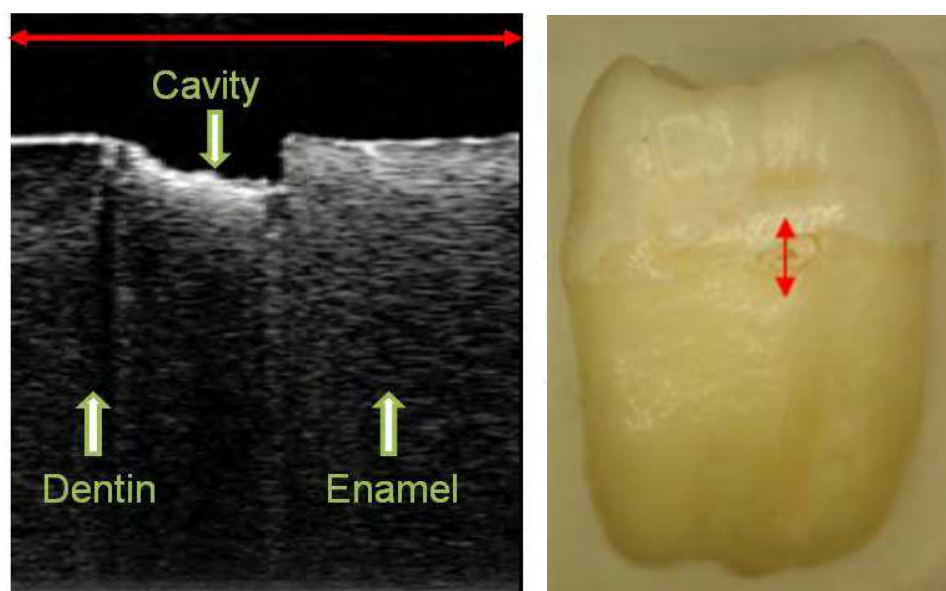


Fig. 3. An OCT B-scan frame from buccal orientation scanning across a hole about 1mm diameter on the surface near the cementoenamel junction line. We scanned across the lesion for about 4 mm in lateral length. The image depth is also about 4 mm. The scanning range is indicated with red arrows on the OCT image and the tooth photo. OCT image clearly shows stronger scattering from the lesion area.

### 3.2 Polarization-sensitive dental OCT

OCT is capable of coherence detection of polarization states from the backscattered signal. Dental tissue happens to be very sensitive to light polarization. Therefore more detection information can be obtained by polarization sensitive OCT (PS-OCT). Literatures have shown strong evidence that PS-OCT significantly enhances the detection power of OCT. In dental OCT, polarization is a metric parameter that may not be overlooked. It is because enamel and dentin as the primary components of human teeth, have shown interesting polarization effects. The effect can be used to evaluation the tooth structure. It is also because a polarization sensitive OCT imaging scheme is not deployed, the polarization effect could come back as strong polarization artifacts to distort the true structural information even in a regular intensity OCT.

Figure 4 shows the polarization sensitive system developed to produce the PS-OCT image results in this chapter. The polarization response can be calculated based on the Jones matrix formalism. The complex light field is expressed as a vector of vertical and horizontal parts:

$$\mathbf{E} = \begin{pmatrix} \tilde{E}_V \\ \tilde{E}_H \end{pmatrix} \quad (1)$$

V and H indicate the two orthogonal polarization directions. ,  $E_V$  and  $E_H$  are the detected field amplitude. The polarization effect of the sample to the light can be expressed in a general retarder form as

$$S(\phi, \theta) = \begin{pmatrix} \cos^2 \theta + \sin^2 \theta \cdot e^{-j2\phi} & \cos \theta \cdot \sin \theta \cdot (1 - e^{-j2\phi}) \\ \cos \theta \cdot \sin \theta \cdot (1 - e^{-j2\phi}) & \cos^2 \theta \cdot e^{-j2\phi} + \sin^2 \theta \end{pmatrix} \quad (2)$$

where  $\phi$  is the average phase retardation angle (single trip of back scattered photon) and  $\theta$  is the average fast axis orientation. Following this Jones matrix formalism, we have in the standard CP configuration:

$$\tilde{E}_V = A_V \exp [-(\Delta z / l)^2] \sin(\phi) \exp(-i\phi) \quad (3)$$

$$\tilde{E}_H = A_H \exp [-(\Delta z / l)^2] \cos(\phi) \exp[-i(\phi+2\theta-\pi)] \quad (4)$$

where  $\Delta z$  is the optical path difference and  $l$  is the SLD coherence length. Since the two channels are identical, constants  $A_V$  and  $A_H$  can be considered to be the same. The phase retardation  $\phi$  can then be expressed by

$$\phi = \arctan (E_V/E_H) \quad (5)$$

The phase retardation values vary from 0 to 90 degree. The regular OCT image can be obtained by

$$E_{oct} = \text{sqrt}( E_V^2 + E_H^2 ) \quad (6)$$

Detailed Jones' formalism calculation can be found from other papers<sup>57, 58</sup>.

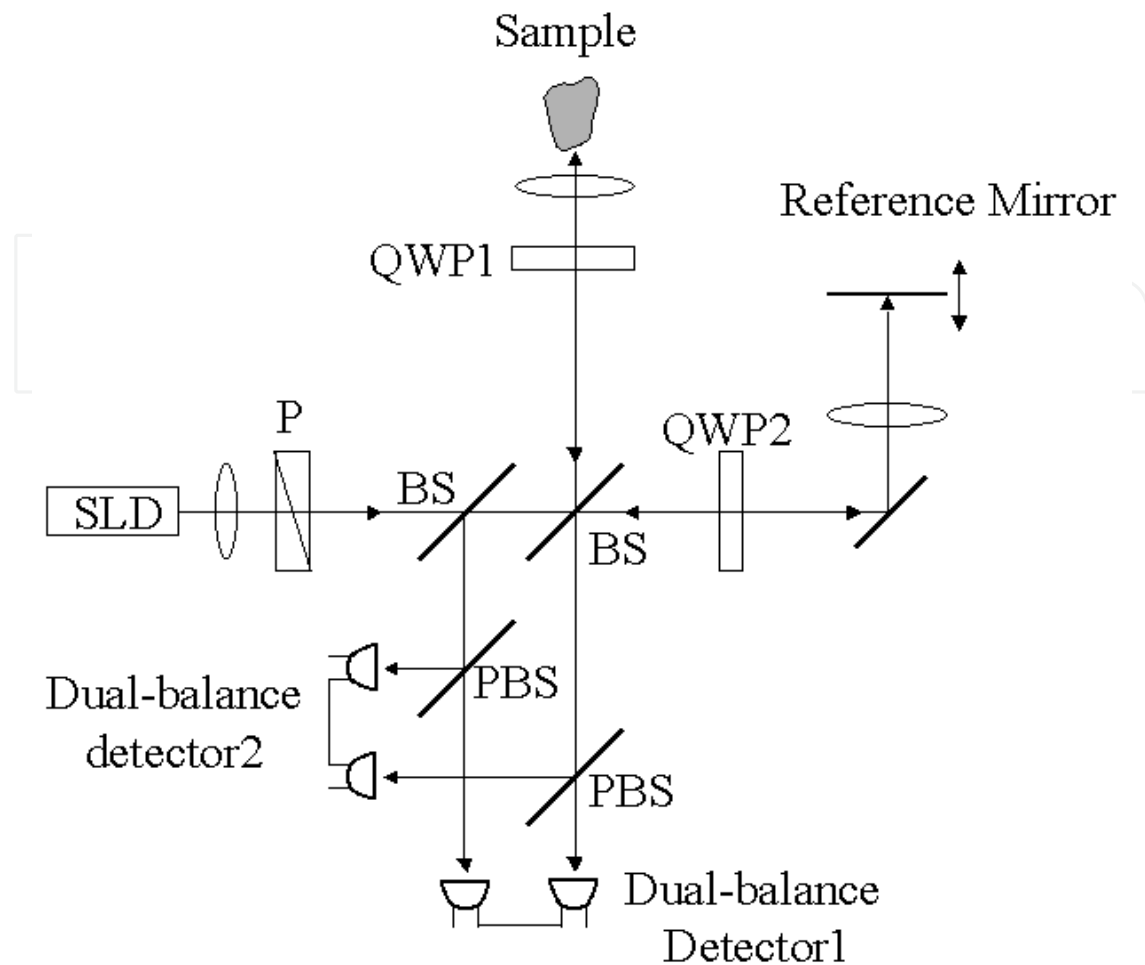


Fig. 4. Schematic of the PS-OCT system. SLD, superluminescent diode; P, polarizer; BS, beam splitter; PBS, polarizing beam splitters; QWP1, QWP2, quarter-wave plates; Galvo, galvanometer.

We'd like to point out that in PS-OCT two-channel detection is required. This increases the data volume and the complicity of data processing. There are subsequently more ways to representing the data. Figure 5 shows a generally accepted image construction standard that produces four sets of images. The four images map imaging parameters  $\log(E_V)$ ,  $\log(E_H)$ ,  $\phi$ , and  $\log(E_{oct})$  accordingly. Fig.5A is the cross-polarization channel image. Fig. 5C is called PS-OCT image that maps a physical parameter of the phase retardation (0 to 90 degree angle). Fig. 5D is regular intensity OCT image. It will be approximate to the co-polarization or horizontal channel image in Fig. 5B, if the polarization effect is not strong.

Figure.5 shows the enamel structure and the well-delineated DEJ scanned from the facial aspect. The image size is 2.5mm in lateral and 3.6mm in depth (the depth in air, with no index modification). In Fig.5A, B, and D, DEJ can be identified as a white interface due to its strong reflection. The DEJ is differentiated as a line of texture pattern in phase retardation image shown in Fig. 5C. The penetration depth of dentin is generally found to be less than that of enamel. Images of enamel generally have richer information and deeper penetration, while images in dentin usually have a shallower depth profile. Two types of tissues can be clearly differentiated by their scattering properties.



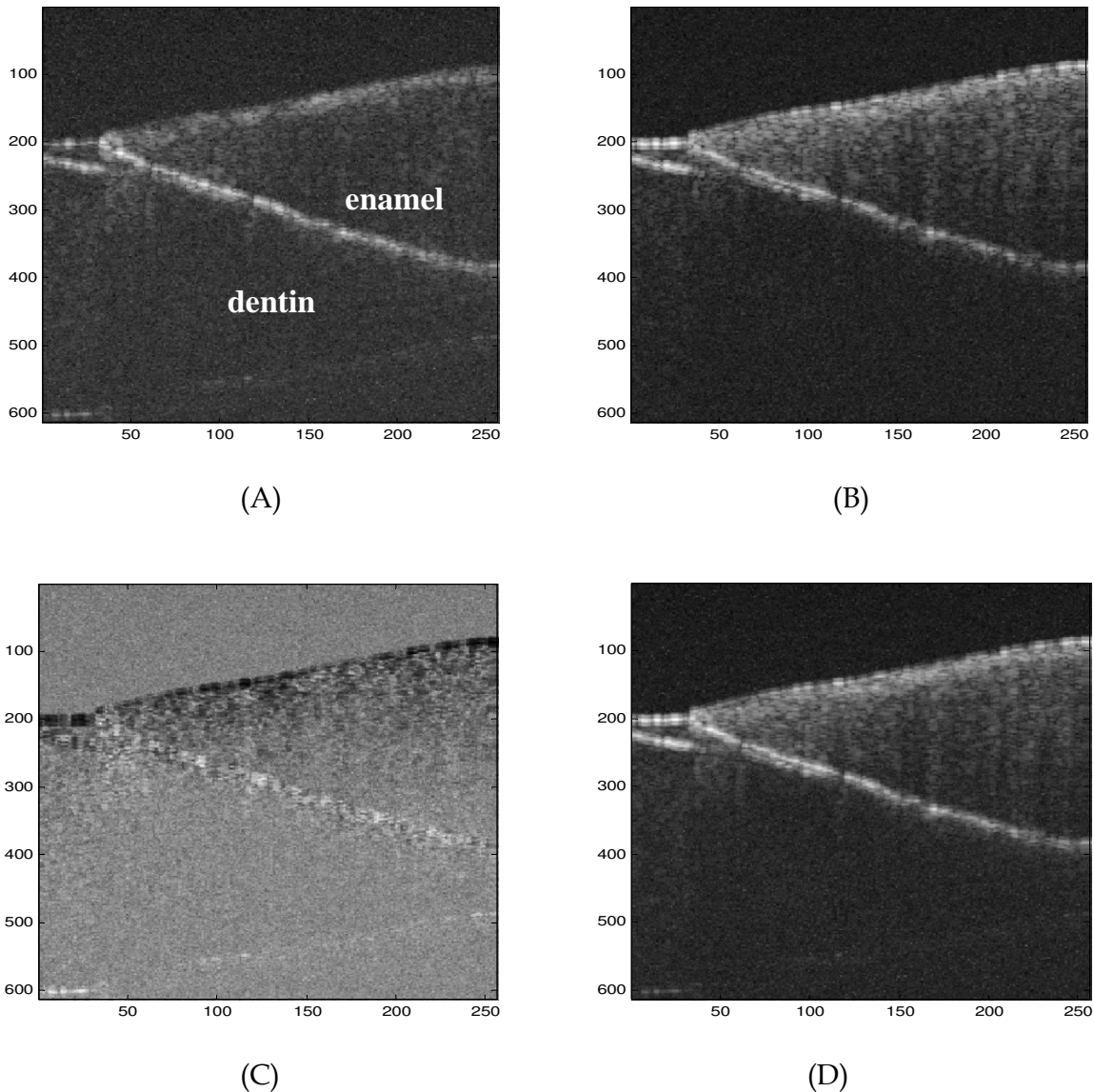


Fig. 5. (A), V-channel image. (B), H-channel image. (C), Polarization sensitive image by  $\phi = \arctan(E_V/E_H)$ . (D), Intensity image by  $R = E_V^2 + E_H^2$ . The bright reflection band inside is the DEJ and towards surface on the left, the cementum boundary can be visualized too.

To measure the polarization sensitivity in dental matrix and its correlation to demineralization, Fried et al.<sup>59</sup> found to assess cross-polarization channel image are already satisfying. The PS-OCT images using the phase retardation brings more comprehensive information. It is well suited to evaluate the biophysical phenomenon of birefringence.

### 3.2.1 PS-OCT image birefringence in enamel

We prepared several excised human teeth that had no visible evidence of caries to study the dental structure. And several tooth samples with caries that can be visually identified in occlusal and interproximal regions were imaged to characterize carious lesion properties. The structural features of enamel were evaluated from the interproximal, facial, and occlusal aspects of the intact human teeth with and without visible caries evidence. For the

assessment of dentin structural features, some teeth were also sectioned in a mesial to distal orientation and in a coronal orientation to image the underneath dentin tissue.

Figure 6 shows images from the interproximal (A) and occlusal aspects (B) of two tooth sample. The global birefringent properties of enamel arises from the regular orientation of the enamel rods. Enamel rods originate at the DEJ in a perpendicular orientation, after a short distance they turn in a plane horizontal to their long axis, first in one direction and then the other until they assume a straight alignment perpendicular to the surface. In longitudinal microscopic ground sections viewed with reflected light, this arrangement of the enamel rods gives rise to a light and dark pattern termed Hunter-Schreger bands. Our results indicate that Hunter-Schreger bands can be seen in PS-OCT of Figure 6A. This morphology is consistent with that previously described in light microscopic images. It is interesting to note that the curvature of the horizontal black-and-white alternating band (the form birefringent bands) aligns normally with the structure of the enamel rods, which implies a relationship of the form birefringence with the ordered spatial structures. The diameter of a single enamel rod is smallest at the DEJ and increases towards the surface. The average diameter of a single rod is about  $4 \mu\text{m}$  while the PS-OCT limit is  $5 \mu\text{m}$  /pixel. High resolution OCT should provide further definition to the study human enamel rod microstructure. Incremental growth lines of enamel (lines of Retzius) have been described in light microscopic images of teeth. When viewed in coronal sections, the lines of Retzius are seen as parallel concentric circles similar to the growth rings on a tree, in longitudinal sections they appear oblique to the surface. The lines of Retzius are typically less prominent at the cervical aspect of the crowns. In PS-OCT images from the coronal aspect of enamel, we have observed alternate black-and-white bands that are consistent with the line of Retzius in most of the teeth imaged in this study. The form birefringence from the coronal aspect is generally stronger than that from the cervical aspect.

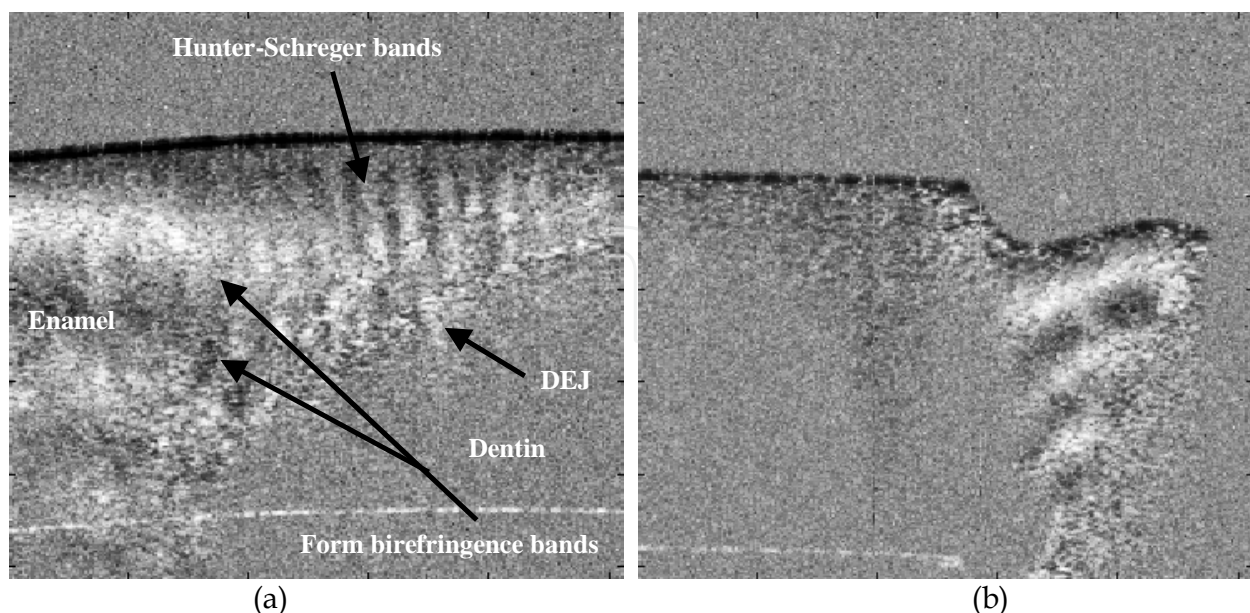


Fig. 6. The phase retardation image from the interproximal aspect. The horizontal black-and-white band structure is originated from the form birefringence. The image size is 2.6mm x 3.6mm (W x H).

Both dentin and enamel show local polarization-sensitive textures. These textural patterns are formed by PS particles about 20~100 micron in diameters. We put an emphasis on this feature because the textures reveal non-invasively rich information underneath the tooth surface. Systematic analysis of these textures such as particle size, polarization strength, orientation and distribution of the patterns etc. may correlate to the mineralization status of the teeth. As dental caries results from a gradual demineralization of enamel and underlying dentin, the mineralization level is an important indicator for the extent of the carious lesions.

Figure 7 shows images with occlusal and interproximal carious lesions. The carious site can be identified as phase retardation texture pattern, which exhibit the strong local polarization sensitive scattering. This type of pattern was seen frequently around carious region. The carious lesions show richer texture information and higher contrast than non-carious site. The pattern is characterized by randomly distributed spots in black and white, which exhibit the strong local polarization sensitive scattering. Occlusal carious lesion is showed in the top figure of Fig. 7, and the caries area is emphasised in the rectangular area with a white arrow points toward the carious site. The areas indicated by black arrows 1 and 2 show similar caries patterns but no caries can be visually identified at the corresponding surfaces. These areas may indicate the boundary of early caries progression that can not be directly identified by eyes yet. The white bands in area 3 and 4 indicate that the energy is preserved in V channel through a deep depth. These areas have textures made of spots with similar size as in caries site but the state of polarization tends to be maintained, i.e. white always appears white and black always appears black. This type of pattern was seen frequently around carious region. Similar features are found also when the images is taken from the interproximal aspect as see from the bottom image of Fig. 7.

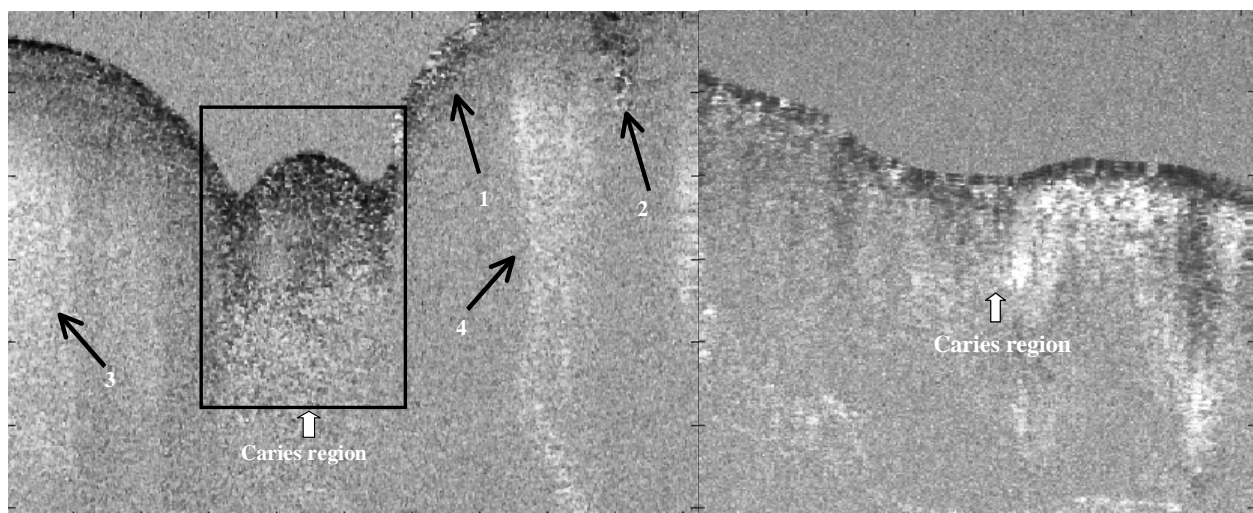


Fig. 7. The local polarization sensitive patterns in the phase retardation images of the tooth samples may closely relate to the mineral composition, which is an indicator of the carious affections. The upper image shows the occlusal carious lesion and the lower one images the lesion from the interproximal aspect as marked by white arrows.

Besides the imaging from the outer surface of the extracted tooth samples, we also imaged the interior aspect of sectioned teeth. In Fig. 8, we show two long PS-OCT scans about 1 cm in lateral length. The imaging depth is also 3.6 mm. The separation of dentin and enamel

and their different polarization sensitive scattering properties are well delineated. In the bottom figure, the circled dark area may be associated with demineralization.

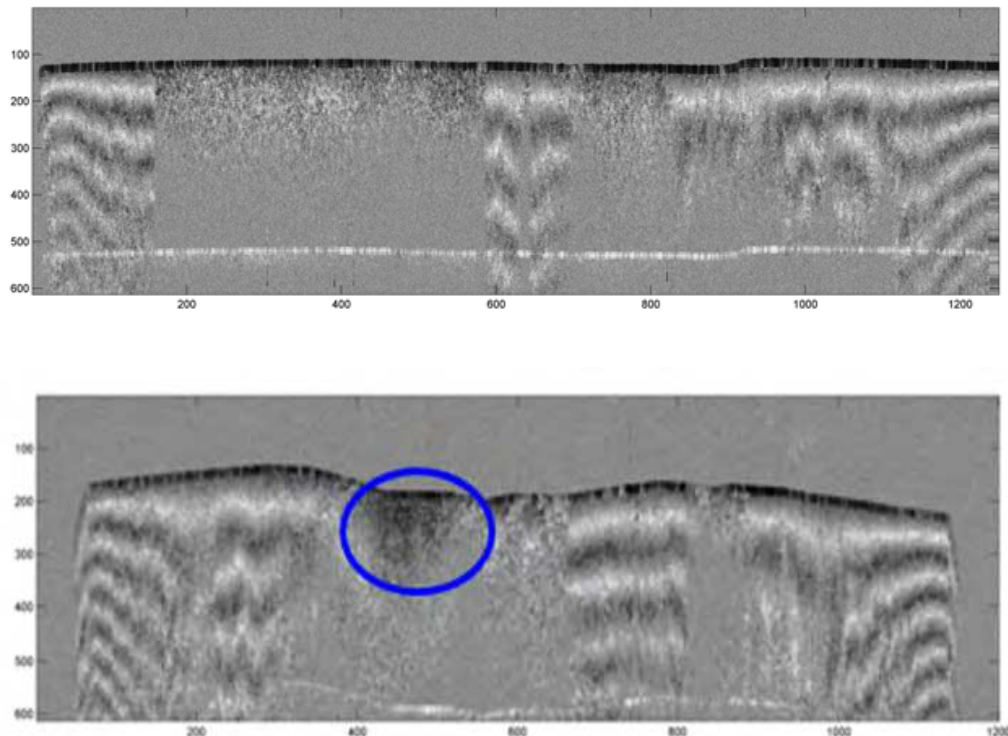


Fig. 8. Phase retardation image from the interior of sectioned tooth samples. The image size is about 10 mm x 3.6mm. The circled area from the bottom image reveals a dark spot, which may be associated with strong demineralization.

In summary, this section discussed the use of PS-OCT imaging to characterize dentin and enamel, and to study the special properties related to the structural orientation of enamel rods. We have performed imaging experiment for more than one hundred tooth samples of different age groups, healthy and carious, from human and animal. The results show that teeth are strong polarization-sensitive tissues. As a general comparison with the conventional intensity OCT, the PS-OCT images provide a unique contrast and could relate to functional information such as demineralization. The polarization detection capability should be regularly applied for OCT system to fully characterize the scattering information of dental tissues.

### 3.2.2 Polarization memory effect in dentin

Polarization memory describes a phenomenon whereby light retains its incident polarization state after it is back-scattered from a turbid medium<sup>60</sup>. When polarization memory effect (PME) is discussed, it is more convenient to define the two polarization channels by cross-polarization (x-pol) and co-polarization (co-pol) rather than physically the vertical and horizontal channels. In 3.2.1 section, the vertical channel is the x-pol channel, because this channel conventionally won't receive a big amount of photon signal unless there exists a significant polarization sensitive scattering mechanism in the tissue sample.

We will skip some lengthy maths and theory about PME for which readers can find from the authors' recent work <sup>41, 42</sup>. A simpler picture is PME happens when the back scattering circularly polarized light **remembers** the original helicity. As a result a significant amount of light power will be detected from the conventionally very weak x-pol channels. Because of the polarization memory, the light field energy is transferred from the co-pol channel to the x-pol channel and sometimes it results in signal strength reversal between the two channels. In this context, a cross-polarization discrimination (XPD) ratio is conveniently defined to tell us how much photon energy has leaked to the x-pol. Channel due the polarization effect of the tissue.

$$\text{XPD}(z) = 20 \log (E_{\text{x-pol}}(z) / E_{\text{co-pol}}(z)) \quad (7)$$

XPD and phase retardation angle have clear physics meanings for PME and birefringence, respectively. From the imaging prospective, the two terms give different mapping functions in PS-OCT. The XPD is defined to map the PS-OCT images in this section. Visually, it does not appear very different. The PS-OCT images in Fig. 9 for example looks much alike what we see in Fig. 8. XPD is however bears a clearer meaning in order characterizing and quantifying PME. PME is a relatively weak polarization effect and was found in dentin rather than in enamel. We will however, try to correlate the result with subtle demineralization process that is the sign of tooth decay.

To design this study, demineralization drug was used to create artificial cavities. 5 teeth were sectioned in an axial orientation. 37% phosphoric acid gel was placed on the sectioned dentin surface for 60 seconds and then washed away. This "acid conditioning of a dentin surface" produced micromorphological effects on the dentin surface, removing the organic material within the surface dentinal tubule orifices, as previously shown <sup>29</sup>. In other words after the gel was placed on the tooth, the surface dentin composed of tubules of mineral hydroxylapatite could lose a significant amount of organic material. Subsequently, OCT scans were taken across the enamel and the mantel dentin. The lesion region had a slight brownish hue which was helpful in steering the OCT beam through the target.

PME is seen in the averaged XPD lines of tooth samples for example in Fig. 9 A. The red line averages the drug affected region and the blue line averages the normal region. Before averaging, the XPD line was realigned along the dentin-air surface with an edge detection algorithm. According to the definition of XPD ratio in Eq. 7, when the blue line is larger than 0, it indicates a stronger x-pol channel signal strength than the co-pol channel, which usually is the dominating channel in signal strength. Therefore our result suggests that the normal dentin area, i.e. without demineralization drug treatment shows polarization memory. The result is a quick increase in x-pol channel signal strength as light travels inside the dentin as shown with the blue curves. The signal strength of x-pol channel exceeds the signal strength of co-pol channel as much as 80%. This is rarely happening unless a significant polarization effect is taken place. For the drug processed artificial cavity region, however, this significant memory effect disappears. The red curve appears to be gradually approach zero line when going into noise floor at deeper depth. Same effect is also seen in Fig. 9B. Only one sees the red curve rises above the zero line too, but at a deeper depth. This should be due to the limited progressing depth of the demineralization drug. The two black arrows point zero crossing points of the blue and the red curve at two different depth. It is interesting to see that after the second depth, the red XPD line seems to regain its polarization memory. The

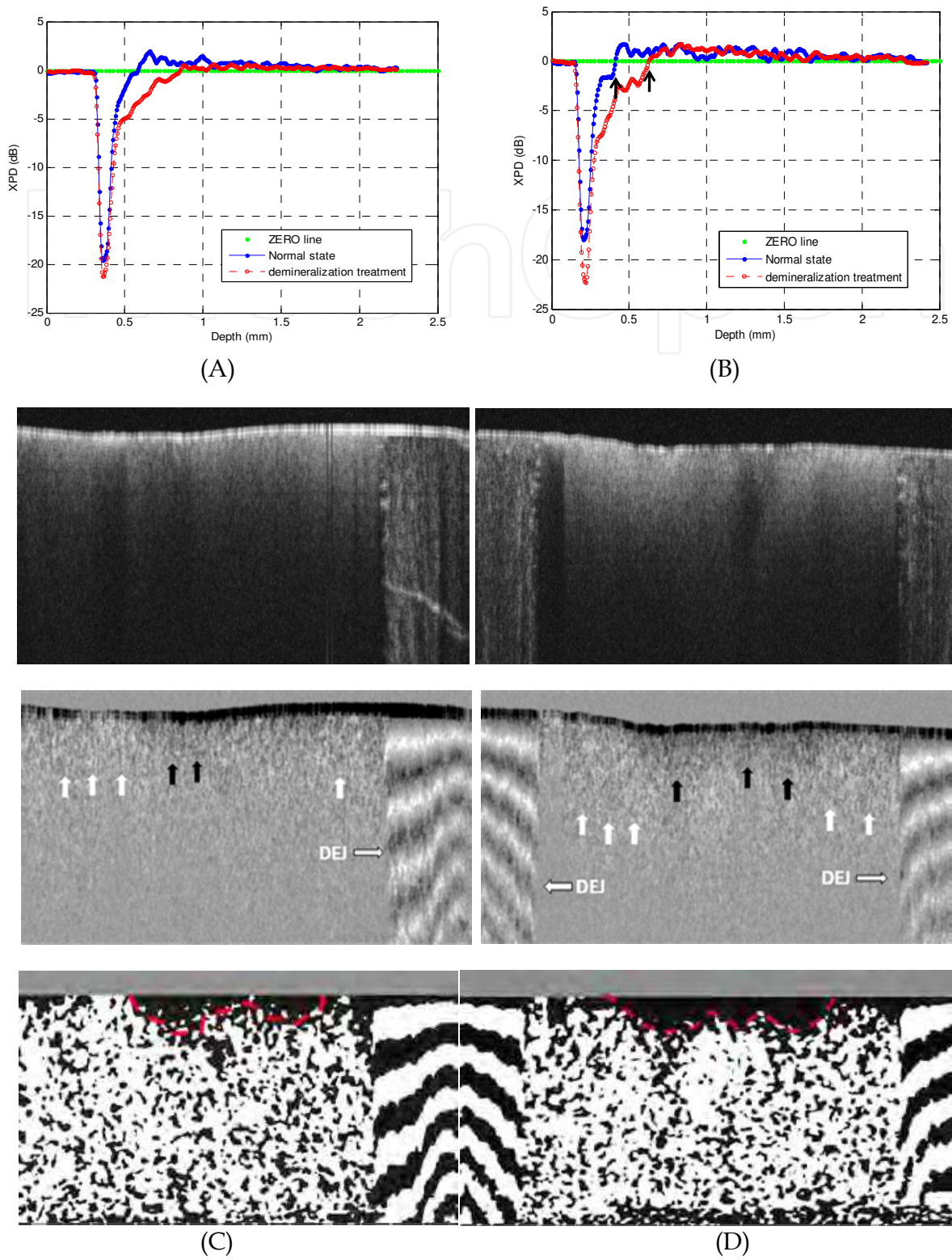


Fig. 9. Two tooth samples imaged after demineralization process. The image size is about 3.2x 8mm in air. (A) and (B) are the averaged XPD curves from treated (red) and intact (blue) area. (C) and (D) show the OCT intensity images (top), the PS-OCT images mapped by XPD lines(middle), and the binary images (bottom) with a better visualization of the progression of the demineralization treatment.

distance between the two arrows roughly indicates the progression of the demineralization treatment. Fig.9 C and D show the two corresponding OCT scans across both the dentin and the adjacent enamel. The regular intensity OCT images are shown at the top. The PS-OCT images mapped by XPD lines in the middle show the different imaging features of dentin and enamel due to the two different polarization behaviours: the alternate bright and dark bands on the right side of Fig. 9C and on both sides of Fig. 9D are typical features of birefringence in the enamel, while the dim single white band in the middle is a feature from PME in the dentin. DEJ, the junction between dentin and enamel identified as a vertical border clearly splits the two types of tissues which are much less separable in the intensity mapped OCT images. Birefringence is a well acknowledged effect in PS-OCT. PME is still new and will be examined more by future studies. Both effects could lead to useful medical applications. The middle parts of the PS-OCT images near the surface corresponded to where the phosphoric acid process was applied. These areas appear darker which imply that some polarization memory is lost. PME can be better estimated through averaging and other filtering processing with a penalty in spatial resolution. Furthermore, PME quantified by XPD ratio has a characteristic zero line which can serve as a sensitive benchmark for spatial demarcation of dematerialized and normal dentin tissue. The bottom images of Fig. 9 C and D are the processed binary images using zero XPD level as the threshold to enhance the contrast. It can be seen that the energy in cross-polarization channel exceeds that in co-polarization channel in most part of the dentin images except the dark areas near the middle of the dentin surface. Estimated spatial boundaries of acid progression are drawn in red dashed lines. A 5x5 medium filter and a 3x3 linear statistical de-speckle filter were used before the binary image process to reduce speckle noise.

In summary, we have discussed in this section a new type of polarization effect, PME that may help to diagnose decay in dentin tissues. As a follow-up future research work, it would be interesting to extend the study to the remineralization study to evaluate the efficacy of rehabilitation drugs. As a blind test, two tooth pastes with one plain (expected to do nothing) and the second containing for example, amorphous calcium phosphate that expected to put mineral back into the etched dentin can be used. PS-OCT using PME analysis may prove to be a useful *in vitro* method to evaluate the efficacy of drugs for repairing dental caries in addition to the potential application for the early caries detection. This remineralization and demineralization testing may be applied on extracted teeth repeatedly without the need to destroy them for investigation such as in the case of optical or electron microscopic imaging.

From the technology prospective, this study was performed with a less sensitive time-domain OCT. It would be helpful to use a 3D imaging protocol with more sensitive Fourier-domain OCT technology to study the changes before and after mineralization treatment. In this way, the tissue locations can be registered for more accurate comparison.

#### **4. 3D and high dimensional imaging and multimodality registration**

Fourier domain OCT (FD-OCT) with high speed and sensitivity makes it feasible for real-time 3D imaging. Towards the future development and application of OCT technology, 3D dental imaging enables registration of OCT to itself at different time points and therefore becomes 4D imaging modality. Moreover, once the 3D imaging structure is scanned, the OCT scans can be registering or fusing to other dental image modalities, for example, 3D micro CT scans.

Figure 10 shows the 3D imaging results of a molar tooth from the occlusal surface. The topology of tooth surface is clearly seen. The pit area is where a majority of caries affection occurs which is also hard to be detected by dental X-ray. The scan has a depth resolution about  $10\ \mu\text{m}$  in tissue assuming optical index of 1.38. The imaging volume consists of 60 frames (B-scans) each with 150 axial scan lines (A-line). With our scanner, image is acquired at a frame rate of 60 fps. Therefore the total time to acquire this 3D dataset is only one second. The lateral scanning area is about  $10\ \text{mm} \times 10\ \text{mm}$  basically covering the full surface area along the occlusal orientation. We also selected 3 typical B-scans to the left side of Fig.10. The imaging depth in air is about 3 mm. These B-scans reveals micron scale fine resolution of tooth structures, where the contrast is from optical scattering of small particles and interfaces.

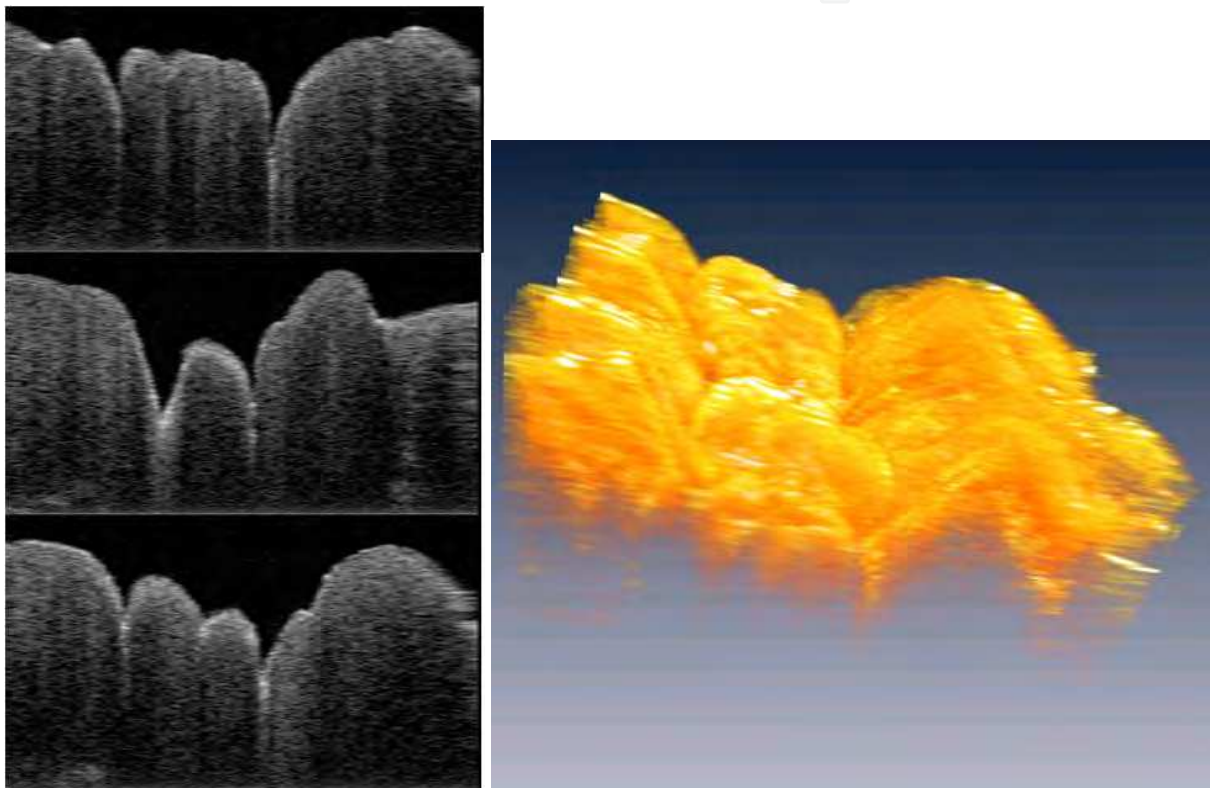


Fig. 10. Three dimensional volumetric imaging and three typical B-scan frames of a molar tooth ex vivo using FD-OCT.

3D imaging brings flexibility to view data from multiple angles such as regular tomographic B-scan frame, slow frame, and *en face* imaging similar to microscopy. 3D OCT can also generate projection image along multiple axes too. This is demonstrated in the bottom right images in Fig. 11, where a 3D rendering of acquired OCT data is overlaid with projections from fast axis and slow axis. We would also have maximal freedom to view projections along any arbitrary projectile directions. In the top left image of fig. 11, we intend to bring some comparisons between 3D OCT and X-ray, although this is not a strict sense apple-to-apple comparison, we could directly appreciate the enhanced resolution and contrast from OCT projections on top-left compared to the X-ray projection on right. 3D imaging helps image registration of frame locations through correlations of the topological features to other detection such as photo picture or X-ray images. The red rectangles enclosed the OCT



projectile imaging and X-ray projections are roughly matched in spatial location. Typically, dental expert will enhance the contrast of the X-ray image and look for a delicate trace of darker shade as an indication of tooth decay. This is a difficult metric that requires well trained eyes. The exact location of decay is uncertain. Many cavity lesions are left unnoticed. The OCT projection appeared to have better resolution and contrast. But future study may find that it may not be the OCT way to identify cavities. Likely scattering patterns in PS-OCT and intensity or slope changes in intensity OCT could prevail to be the better biomarkers to demark the lesion regions.

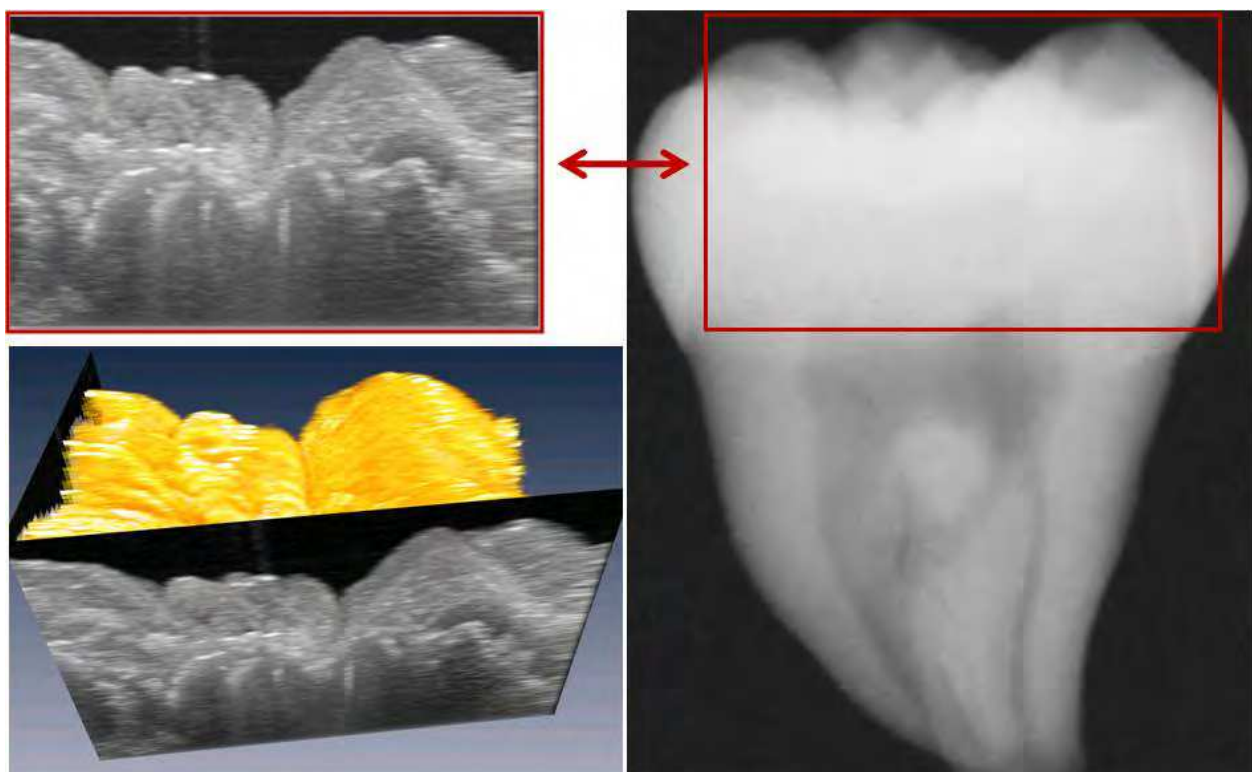


Fig. 11. Top left: OCT projection image roughly matched to the X-ray scan to the right. Bottom left: with 3D OCT, multiple projections can be assessed with a single dataset.

Figure 12 shows a another 3D scan from interproximal prospective. Beside a smoother tooth surface compared to occlusal orientation, it is notable we can clearly visualize boundary features of the dentin-enamel junction. 3D OCT enables a direct visual investigation of the two primary calcified components of tooth and their 2D boundary structure *in vivo*. In the top-left figure, we interleaved the DEJ topology from the tooth matrix. It appears to have a couple of holes which is also identified as discontinuities in the corresponding B-scans in the bottom pictures. We note that X-ray is much capable in finding interproximal tooth decay and it is actually more difficult for OCT to scan the tissue area in between the teeth. In this sense, conventional X-ray and new dental OCT imaging may benefit and complimentary from each other.

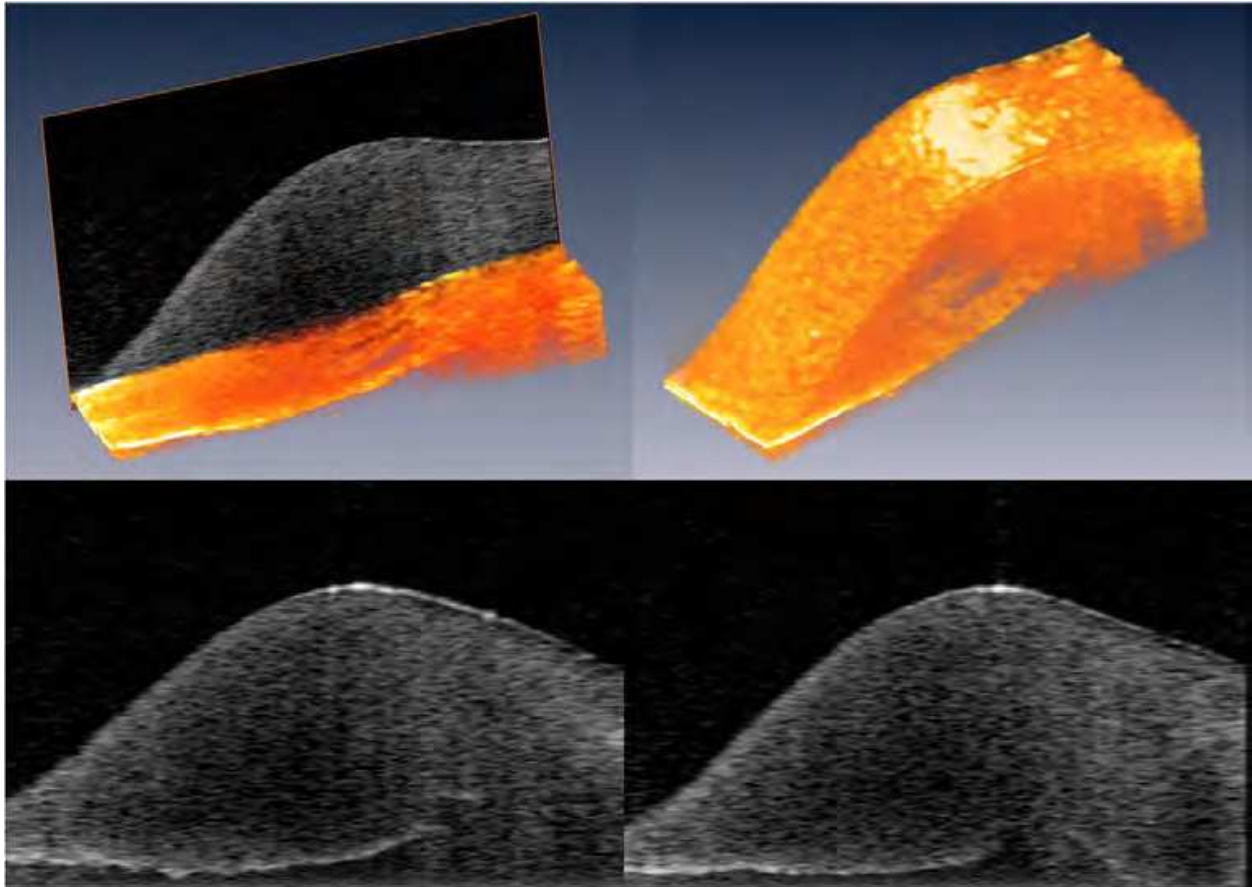


Fig. 12. A three dimensional OCT scan from the interproximal prospective. It goes with the same scanning protocol as in Fig. 10. The top-left image removes some tissue to reveal the 2D DEJ topology. The top-right imagerenders the tooth surfaces. The bottom images are two sample frames of the OCT B-scans. 3D-OCT sometimes is called C-scan. A-scan, B-scan, and C-scan are borrowed from the existing ultrasound imaging terms.

## 5. Summary

The results of this study indicate that OCT and PS-OCT has the promising sensitivity to the physiologic and pathogenic changes of dentin and enamel unavailable by current diagnostic or imaging methods. It has the potential to be used for both dental research and clinic applications. As a relatively inexpensive and non-invasive system with high depth resolution, PS-OCT also has the capability of 3D imaging for caries detection. Additional studies that correlate the changes in PS-OCT ultrastructural features that occur in demineralization should provide important information regarding the usefulness of this technology for the clinical diagnoses of dental caries. Since the different texture patterns are most likely related to the mineral components within the tooth, it is interesting and promising to design dynamic processes with demineralization, remineralization and acid control to track the relation between mineralization level and PS-OCT features. The change of the texture patterns before and after treatment can be potentially monitored and compared. Dynamic experiments may prove to be a sensitive way to quantitatively assess the microstructural components in the tooth. It is a prior knowledge of these features and their relations with mineralization level that will provide verification of the diagnostic

power of PS-OCT for caries and pre-carious lesions. Ultimately, clinical trials must be completed to study the sensitivity, specificity and the accuracy of OCT for dental caries diagnosis.

In the future, we expect that 3D-OCT with the polarization sensitivity will have the potential to become a powerful diagnostic tool in dental clinic. It is partially because OCT has several imaging properties including resolution, contrast, and image orientation that happens to be complimentary to some limitations of X-ray. Future clinic may see multiple-modality and co-registered imaging with X-ray, OCT, and other approaches such as fluorescent imaging for early lesion detections. 3D-OCT may also serve as a non-invasive research tools to study dynamic demineralization and remineralization process. The result can be compared with micro CT, an *in vitro* dental image standard.

## 6. Reference

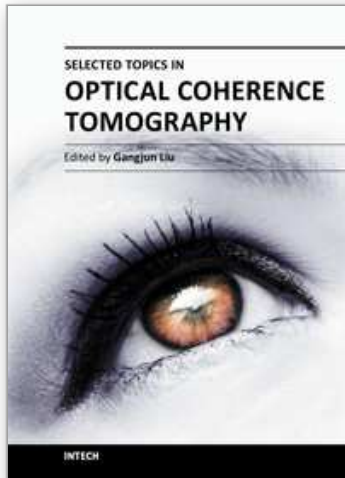
- [1] A. F. Fercher, W. Drexler, C. K. Hitzenberger and T. Lasser, "Optical coherence tomography-principles and applications," Reports on Progress in Physics 66(2), 239-303 (2003)
- [2] M. Wojtkowski, R. Leitgeb, A. Kowalczyk and A. F. Fercher, "Fourier domain OCT imaging of the human eye in vivo," Proc. SPIE 4619(230-236 (2002)
- [3] M. A. Choma, M. V. Sarunic, C. H. Yang and J. A. Izatt, "Sensitivity advantage of swept source and Fourier domain optical coherence tomography," Optics Express 11(18), 2183-2189 (2003)
- [4] G. J. Tearney, B. E. Bouma and J. G. Fujimoto, "High-speed phase- and group-delay scanning with a grating-based phase control delay line," Optics Letters 22(23), 1811-1813 (1997)
- [5] R. A. Leitgeb, L. Schmetterer, C. K. Hitzenberger, A. F. Fercher, F. Berisha, M. Wojtkowski and T. Bajraszewski, "Real-time measurement of in vitro flow by Fourier-domain color Doppler optical coherence tomography," Opt Lett 29(2), 171-173 (2004)
- [6] R. Huber, K. Taira, M. Wojtkowski and J. G. Fujimoto, "Fourier Domain Mode Locked Lasers for OCT imaging at up to 290kHz sweep rates," in Optical Coherence Tomography and Coherence Techniques II W. Drexler, Ed., pp. 245-250, SPIE and OSA, Munich (2005).
- [7] V. J. Srinivasan, M. Wojtkowski, A. J. Witkin, J. S. Duker, T. H. Ko, M. Carvalho, J. S. Schuman, A. Kowalczyk and J. G. Fujimoto, "High-definition and 3-dimensional imaging of macular pathologies with high-speed ultrahigh-resolution optical coherence tomography," Ophthalmology 113(11), 2054-2065 (2006)
- [8] Y. Yasuno, T. Endo, S. Makita, G. Aoki, M. Itoh and T. Yatagai, "Three-dimensional line-field Fourier domain optical coherence tomography for in vivo dermatological investigation," Journal of biomedical optics 11(1), 7 (2006)
- [9] Y. Park, T. J. Ahn, J. C. Kieffer and J. Azana, "Optical frequency domain reflectometry based on real-time Fourier transformation," Optics Express 15(8), 4597-4616 (2007)
- [10] C. A. Puliafito, M. R. Hee, C. P. Lin, E. Reichel, J. S. Schuman, J. S. Duker, J. A. Izatt, E. A. Swanson and J. G. Fujimoto, "Imaging of macular diseases with optical coherence tomography," Ophthalmology 102(2), 217-229 (1995)

- [11] W. Drexler, U. Morgner, R. K. Ghanta, F. X. Kartner, J. S. Schuman and J. G. Fujimoto, "Ultrahigh-resolution ophthalmic optical coherence tomography. [erratum appears in *Nat Med* 2001 May;7(5):636.]," *Nature Medicine* 7(4), 502-507 (2001)
- [12] S. G. Schuman, E. Hertzmark, J. G. Fujimoto and J. S. Schuman, "Wavelength independence and interdevice variability of optical coherence tomography," *Ophthalm Surg Las Im* 35(4), 316-320 (2004)
- [13] V. J. Srinivasan, B. K. Monson, M. Wojtkowski, R. A. Bilonick, I. Gorczynska, R. Chen, J. S. Duker, J. S. Schuman and J. G. Fujimoto, "Characterization of outer retinal morphology with high-speed, ultrahigh-resolution optical coherence tomography," *Investigative ophthalmology & visual science* 49(4), 1571-1579 (2008)
- [14] M. Pircher, B. Baumann, E. Gotzinger and C. K. Hitzenberger, "Retinal cone mosaic imaged with transverse scanning optical coherence tomography," *Optics Letters* 31(12), 1821-1823 (2006)
- [15] E. Gotzinger, M. Pircher, W. Geitzenauer, C. Ahlers, B. Baumann, S. Michels, U. Schmidt-Erfurth and C. K. Hitzenberger, "Retinal pigment epithelium segmentation by polarization sensitive optical coherence tomography," *Opt Express* 16(21), 16410-16422 (2008)
- [16] Y. Chen, D. M. de Bruin, C. Kerbage and J. F. de Boer, "Spectrally balanced detection for optical frequency domain imaging," *Optics Express* 15(25), 16390-16399 (2007)
- [17] J. Ho, A. J. Witkin, J. Liu, Y. Chen, J. G. Fujimoto, J. S. Schuman and J. S. Duker, "Documentation of intraretinal retinal pigment epithelium migration via high-speed ultrahigh-resolution optical coherence tomography," *Ophthalmology* 118(4), 687-693
- [18] Y. Chen, L. N. Vuong, J. Liu, J. Ho, V. J. Srinivasan, I. Gorczynska, A. J. Witkin, J. S. Duker, J. Schuman and J. G. Fujimoto, "Three-dimensional ultrahigh resolution optical coherence tomography imaging of age-related macular degeneration," *Opt Express* 17(5), 4046-4060 (2009)
- [19] V. J. Srinivasan, Y. Chen, J. S. Duker and J. G. Fujimoto, "In vivo functional imaging of intrinsic scattering changes in the human retina with high-speed ultrahigh resolution OCT," *Opt Express* 17(5), 3861-3877 (2009)
- [20] S. Chia, O. C. Raffel, M. Takano, G. J. Tearney, B. E. Bouma and I. K. Jang, "In-vivo comparison of coronary plaque characteristics using optical coherence tomography in women vs. men with acute coronary syndrome," *Coronary Artery Disease* 18(6), 423-427 (2007)
- [21] M. Kawasaki, B. E. Bouma, J. Bressner, S. L. Houser, S. K. Nadkarni, B. D. MacNeill, I. K. Jang, H. Fujiwara and G. J. Tearney, "Diagnostic accuracy of optical coherence tomography and integrated backscatter intravascular ultrasound images for tissue characterization of human coronary plaques," *Journal of the American College of Cardiology* 48(1), 81-88 (2006)
- [22] B. E. Bouma, G. J. Tearney, H. Yabushita, M. Shishkov, C. R. Kauffman, D. D. Gauthier, B. D. MacNeill, S. L. Houser, H. T. Aretz, E. F. Halpern and I. K. Jang, "Evaluation of intracoronary stenting by intravascular optical coherence tomography," *Heart* 89(3), 317-320 (2003)
- [23] T. Kubo, T. Imanishi, S. Takarada, A. Kuroi, S. Ueno, T. Yamano, T. Tanimoto, Y. Matsuo, T. Masho, H. Kitabata, K. Tsuda, Y. Tomobuchi and T. Akasaka, "Assessment of culprit lesion morphology in acute myocardial infarction - Ability

- of optical coherence tomography compared with intravascular ultrasound and coronary angiography," *Journal of the American College of Cardiology* 50(10), 933-939 (2007)
- [24] T. Sawada, J. Shite, T. Shinke, S. Watanabe, H. Otake, D. Matsumoto, Y. Imuro, D. Ogasawara, O. L. Paredes and M. Yokoyama, "Persistent malapposition after implantation of sirolimus-eluting stent into intramural coronary hematoma - Optical coherence tomography observations," *Circulation Journal* 70(11), 1515-1519 (2006)
- [25] T. Kume, T. Akasaka, T. Kawamoto, N. Watanabe, E. Toyota, Y. Neishi, R. Sukmawan, Y. Sadahira and K. Yoshida, "Assessment of coronary arterial plaque by optical coherence tomography," *American Journal of Cardiology* 97(8), 1172-1175 (2006)
- [26] M. E. Brezinski, "Optical coherence tomography for identifying unstable coronary plaque," *International Journal of Cardiology* 107(2), 154-165 (2006)
- [27] G. J. Tearney, I. K. Jang, D. H. Kang, H. T. Aretz, S. L. Houser, T. J. Brady, K. Schlendorf, M. Shishkov and B. E. Bouma, "Porcine coronary imaging in vivo by optical coherence tomography," *Acta cardiologica* 55(4), 233-237 (2000)
- [28] J. Weissman, T. Hancewicz and P. Kaplan, "Optical coherence tomography of skin for measurement of epidermal thickness by shapelet-based image analysis," *Optics Express* 12(23), (2004)
- [29] M. C. Pierce, J. Strasswimmer, B. H. Park, B. Cense and J. F. de Boer, "Birefringence measurements in human skin using polarization-sensitive optical coherence tomography," *Journal of biomedical optics* 9(2), 287-291 (2004)
- [30] Y. H. Zhao, Z. P. Chen, C. Saxer, S. H. Xiang, J. F. de Boer and J. S. Nelson, "Phase-resolved optical coherence tomography and optical Doppler tomography for imaging blood flow in human skin with fast scanning speed and high velocity sensitivity," *Optics Letters* 25(2), 114-116 (2000)
- [31] J. Welzel, E. Lankenau, R. Birngruber and R. Engelhardt, "Optical coherence tomography of the skin," *Current problems in dermatology* 26(27-37) (1998)
- [32] A. Baumgartner, S. Dichtl, C. K. Hitzenberger, H. Sattmann, B. Robl, A. Moritz, A. F. Fercher and W. Sperr, "Polarization-sensitive optical coherence tomography of dental structures," *Caries research* 34(1), 59-69 (2000)
- [33] B. W. Colston, Jr., M. J. Everett, U. S. Sathyam, L. B. DaSilva and L. L. Otis, "Imaging of the oral cavity using optical coherence tomography," *Monographs in oral science* 17(32-55) (2000)
- [34] L. L. Otis, B. W. Colston, Jr., M. J. Everett and H. Nathel, "Dental optical coherence tomography: a comparison of two in vitro systems," *Dento maxillo facial radiology* 29(2), 85-89 (2000)
- [35] L. L. Otis, M. J. Everett, U. S. Sathyam and B. W. Colston, Jr., "Optical coherence tomography: a new imaging technology for dentistry," *The Journal of the American Dental Association* 131(4), 511-514 (2000)
- [36] D. Fried, J. Xie, S. Shafi, J. D. B. Featherstone, T. M. Breunig and L. Charles, "Imaging caries lesions and lesion progression with polarization sensitive optical coherence tomography," *Journal of biomedical optics* 7(4), 618-627 (2002)
- [37] L. L. Otis, R. I. al-Sadhan, J. Meiers and D. Redford-Badwal, "Identification of occlusal sealants using optical coherence tomography," *The Journal of clinical dentistry* 14(1), 7-10 (2003)

- [38] A. C.-T. Ko, L.-P. Choo-Smith, M. Hewko, L. Leonardi, M. G. Sowa, C. C. S. Dong, P. Williams and B. Cleghorn, "Ex vivo detection and characterization of early dental caries by optical coherence tomography and Raman spectroscopy," *Journal of biomedical optics* 10(3), 31118-31111 (2005)
- [39] R. S. Jones, C. L. Darling, J. D. B. Featherstone and D. Fried, "Remineralization of in vitro dental caries assessed with polarization-sensitive optical coherence tomography," *Journal of biomedical optics* 11(1), 9 (2006)
- [40] R. S. Jones, C. L. Darling, J. D. B. Featherstone and D. Fried, "Imaging artificial caries on the occlusal surfaces with polarization-sensitive optical coherence tomography," *Caries Research* 40(2), 81-89 (2006)
- [41] Y. L. Chen, L. Otis and Q. Zhu, "Polarization Memory Effect in Optical Coherence Tomography and Dental Imaging Application," *Journal of biomedical optics* 16((2011)
- [42] Y. Chen, L. Otis and Q. Zhu, "Polarization memory effect in the polarization-sensitive optical coherence tomography system," *Proc. SPIE* 6429(6429K), 1-5 (2007)
- [43] Y. Chen, L. Otis, D. Piao and Q. Zhu, "Characterization of dentin, enamel, and carious lesions by a polarization-sensitive optical coherence tomography system," *Appl Optics* 44(11), 2041-2048 (2005)
- [44] K. Hosseini, A. I. Kholodnykh, I. Y. Petrova, R. O. Esenaliev, F. Hendrikse and M. Motamedi, "Monitoring of rabbit cornea response to dehydration stress by optical coherence tomography," *Investigative ophthalmology & visual science* 45(8), 2555-2562 (2004)
- [45] A. Popp, M. Wendel, L. Knels, T. Koch and E. Koch, "Imaging of the three-dimensional alveolar structure and the alveolar mechanics of a ventilated and perfused isolated rabbit lung with Fourier domain optical coherence tomography," *Journal of biomedical optics* 11(1), 9 (2006)
- [46] D. Piao, M. M. Sadeghi, J. Zhang, Y. Chen, A. J. Sinusas and Q. Zhu, "Hybrid positron detection and optical coherence tomography system: design, calibration, and experimental validation with rabbit atherosclerotic models," *Journal of biomedical optics* 10(4), 44010 (2005)
- [47] S. A. Boppart, M. E. Brezinski, B. E. Bouma, G. J. Tearney and J. G. Fujimoto, "Investigation of developing embryonic morphology using optical coherence tomography," *Developmental biology* 177(1), 54-63 (1996)
- [48] M. W. Jenkins, D. C. Adler, M. Gargasha, R. Huber, F. Rothenberg, J. Belding, M. Watanabe, D. L. Wilson, J. G. Fujimoto and A. M. Rollins, "Ultra-high-speed optical coherence tomography imaging and visualization of the embryonic avian heart using a buffered Fourier Domain Mode Locked laser," *Optics Express* 15(10), 6251-6267 (2007)
- [49] W. Luo, D. L. Marks, T. S. Ralston and S. A. Boppart, "Three-dimensional optical coherence tomography of the embryonic murine cardiovascular system," *Journal of biomedical optics* 11(2), 8 (2006)
- [50] J. P. Su, J. Zhang, L. F. Yu and Z. P. Chen, "In vivo three-dimensional microelectromechanical endoscopic swept source optical coherence tomography," *Optics Express* 15(16), 10390-10396 (2007)

- [51] Z. Yaqoob, J. G. Wu, E. J. McDowell, X. Heng and C. H. Yang, "Methods and application areas of endoscopic optical coherence tomography," *Journal of biomedical optics* 11(6), 19 (2006)
- [52] D. Daniltchenko, M. Sachs, E. Lankenau, F. Koenig, G. Huettmann, D. Schnorr, S. Al-Shukri and S. Loening, "Optical coherence tomography of the urinary bladder: The potential of a high-resolution visual investigation technique for endoscopic diagnostics," *Optics and Spectroscopy* 101(1), 40-45 (2006)
- [53] H. Mashimo, S. Desai, M. Pedrosa, M. Wagh, Y. Chen, P. Herz, P. L. Hsiung, A. Aguirre, A. Koski, J. Schmitt and J. G. Fujimoto, "Ultrahigh resolution endoscopic optical coherence tomography: a novel technology for gastrointestinal imaging," *Gastroenterology* 128(4), A251-A251 (2005)
- [54] Y. Chen, P. R. Herz, P.-L. Hsiung, A. D. Aguirre, K. Schneider, J. G. Fujimoto, H. Mashimo, S. Desai, M. Pedrosa, J. M. Schmitt and A. Koski, "Ultrahigh resolution endoscopic optical coherence tomography for gastrointestinal imaging," pp. 4-10, *International Society for Optical Engineering*, Bellingham, WA 98227-0010, United States, San Jose, CA, United States (2005).
- [55] G. J. Tearney, M. E. Brezinski, B. E. Bouma, S. A. Boppart, C. Pitvis, J. F. Southern and J. G. Fujimoto, "In vivo endoscopic optical biopsy with optical coherence tomography," *Science* 276(5321), 2037-2039 (1997)
- [56] D. P. Popescu, M. G. Sowa, M. D. Hewko and L. P. Choo-Smith, "Assessment of early demineralization in teeth using the signal attenuation in optical coherence tomography images," *Journal of biomedical optics* 13(5), 054053 (2008)
- [57] B. H. Park, M. C. Pierce, B. Cense and J. F. de Boer, "Jones matrix analysis for a polarization-sensitive optical coherence tomography system using fiber-optic components," *Optics Letters* 29(21), 2512-2514 (2004)
- [58] J. F. de Boer and T. E. Milner, "Review of polarization sensitive optical coherence tomography and Stokes vector determination," *Journal of biomedical optics* 7(3), 359-371 (2002)
- [59] D. Fried, J. Xie, S. Shafi, J. D. Featherstone, T. M. Breunig and C. Le, "Imaging caries lesions and lesion progression with polarization sensitive optical coherence tomography," *Journal of biomedical optics* 7(4), 618-627 (2002)
- [60] F. C. MacKintosh, J. X. Zhu, D. J. Pine and D. A. Weitz, "Polarization memory of multiply scattered light," *Physical review* 40(13), 9342-9345 (1989)



## **Selected Topics in Optical Coherence Tomography**

Edited by Dr. Gangjun Liu

ISBN 978-953-51-0034-8

Hard cover, 280 pages

**Publisher** InTech

**Published online** 08, February, 2012

**Published in print edition** February, 2012

This book includes different exciting topics in the OCT fields, written by experts from all over the world. Technological developments, as well as clinical and industrial applications are covered. Some interesting topics like the ultrahigh resolution OCT, the functional extension of OCT and the full field OCT are reviewed, and the applications of OCT in ophthalmology, cardiology and dentistry are also addressed. I believe that a broad range of readers, such as students, researchers and physicians will benefit from this book.

### **How to reference**

In order to correctly reference this scholarly work, feel free to copy and paste the following:

Yueli L. Chen, Quan Zhang and Quing Zhu (2012). Optical Coherence Tomography in Dentistry, Selected Topics in Optical Coherence Tomography, Dr. Gangjun Liu (Ed.), ISBN: 978-953-51-0034-8, InTech, Available from: <http://www.intechopen.com/books/selected-topics-in-optical-coherence-tomography/optical-coherence-tomography-in-dentistry>

**INTECH**  
open science | open minds

### **InTech Europe**

University Campus STeP Ri  
Slavka Krautzeka 83/A  
51000 Rijeka, Croatia  
Phone: +385 (51) 770 447  
Fax: +385 (51) 686 166  
[www.intechopen.com](http://www.intechopen.com)

### **InTech China**

Unit 405, Office Block, Hotel Equatorial Shanghai  
No.65, Yan An Road (West), Shanghai, 200040, China  
中国上海市延安西路65号上海国际贵都大饭店办公楼405单元  
Phone: +86-21-62489820  
Fax: +86-21-62489821



© 2012 The Author(s). Licensee IntechOpen. This is an open access article distributed under the terms of the [Creative Commons Attribution 3.0 License](#), which permits unrestricted use, distribution, and reproduction in any medium, provided the original work is properly cited.

IntechOpen

IntechOpen